Superior cycle stability of nitrogen-doped graphene nanosheets as anodes for lithium ion batteries

Xifei Li, Dongsheng Geng, Yong Zhang, Xiangbo Meng, Ruying Li, Xueliang Sun *

Nanomaterials and Energy Lab, Department of Mechanical and Materials Engineering, University of Western Ontario, London, Ontario, Canada N6A 5B9

ARTICLE INFO

ABSTRACT

The specific capacity of nitrogen-doped graphene nanosheet (N-GNS) evidently increases with charge/discharge cycles, exhibiting superior electrochemical performance. N-GNS presented a specific capacity of 684 mAh g^{-1} in the 501st cycles while only 452 mAh g^{-1} in the 100th cycle, accounting for higher cycling stability and larger specific capacity in comparison to a pristine graphene and a commercialized graphite anode. The obtained significant improvement is attributed to the incorporated nitrogen to graphene planes with a result of more structural defects during cycling.

© 2011 Elsevier B.V. All rights reserved.

1. Introduction

Graphene nanosheet (GNS), a new class of two-dimensional carbon allotropes, is structurally different from its precursor graphite [1] and has been attracting great interests since the isolation of a monolayer graphene from layered bulk graphite in 2004 [2]. GNS shows various exceptional properties including ultra-high surface area, high electrical conductivity [3] and high chemical stability [4]. Recent works have shown that GNS exhibited higher capacity than commercialized graphite as anodes for lithium ion batteries (LIBs) [5–8]. All of the aforementioned properties together with low manufacture costs make GNS a promising candidate for LIBs [9].

Doping of heteroatoms into the carbon crystal lattice can tailor both its chemical and physical properties [10,11]. For example, nitrogen-doped carbon nanofibres have metallic characteristic due to the pyridine-like nitrogen and bridgehead-nitrogen [12]. It is reported that the nitrogen-containing polymeric carbon delivered a higher reversible capacity up to 536 mAh g^{-1} due to the effects of nitrogen doping [13]. N-GNS may perform better Li$^+$ storage performance. As it was recently reported by Ajayan et al. [14], N-GNS grown on Cu foil by chemical vapor deposition (CVD) showed almost double reversible capacity compared to pristine graphene. However, CVD can only grow N-GNS thin films on a substrate and thereby suffers from difficulties in scaling up.

In this work, N-GNS was synthesized at a large scale, and exhibited excellent electrochemical performance of Li$^+$ intercalation/de-intercalation. In particular, it is for the first time found that the charge/discharge capacity of N-GNS significantly increases with the charge/discharge cycles before the discharge capacity reaches a maximum value of 684 mAh g^{-1}.

2. Experimental

Natural graphite was oxidized in a modified Hummers method [15] to obtain graphite oxide, as previously reported by our group [16]. Then the received graphite oxide was rapidly exfoliated via a thermal treatment at 1050 °C under nitrogen atmosphere with the product of GNS. GNS was further annealed in the presence of ammonia gas (NH$_3$) and transferred into N-GNS [16,17].

The morphologies of GNS and N-GNS were examined by a field emission scanning electron microscope (Hitachi S-4800), transmission electron microscope (Philips CM10), and high-resolution TEM (JEOL 2010F). Raman spectra were obtained using a Raman spectrometer (Bruker RFS100/S) at a wavelength of 1064.1 nm. XPS analysis was carried out with a Kratos Axis Ultra Al (alpha) X-ray photoelectron spectroscopy operated at 14 kV.

Working electrodes were prepared by slurry casting on a Cu foil. The slurry contained GNS or N-GNS (90 wt.%) and a polyvinylidene fluoride binder (10 wt.%) in N-methylpyrrolidinone (NMP) solvent. A lithium foil was used as a counter electrode. The electrolyte was composed of 1 M LiPF$_6$ salt dissolved in ethylene carbonate: diethyl carbonate: ethyl methyl carbonate in a 1:1:1 volume ratio. Cyclic voltammetry tests were performed on a CHI electrochemistry workstation at a scan rate of 0.1 mV s^{-1} over a potential range of 0.01 to 3.0 V (vs. Li$^+$/Li) at room temperature. Charge–discharge characteristics were tested galvanostatically in a voltage range of

---

* Corresponding author.
  E-mail address: xsun@eng.uwo.ca (X. Sun).

0.01–3.0 V (vs. Li$^+$/Li) at a current density of 100 mA g^{-1} using an Arbin BT-2000 Battery Test System.

3. Results and discussion

The morphologies of GNS and N-GNS are shown in Fig. 1. The FE-SEM image of bulk GNS at low magnification in the inset of Fig. 1a shows that the loose GNS tend to overlap and stick together to form fluffy agglomerates with a worm-like appearance. An increased magnification in Fig. 1a reveals that a "worm" consists of many ultrathin nanosheets with wavy structures. A typical TEM image of GNS in Fig. 1c exhibits characteristic transparent gossamer sheets including only a few graphene layers. The GNS are entangled with each other and scrolled. From Fig. 1b and d, it is obvious that N-GNS also has a rippled and crumpled structure. XPS result indicates that N-GNS contains 2.8 at% nitrogen. As shown in Fig. 1e, the N 1 s signal

splits into three peaks at 398.1, 399.9 and 401.3 eV corresponding to three types of doping nitrogen, i.e. pyridine-like, pyrrole-like and graphitic nitrogen [18]. The Raman spectra of GNS and N-GNS are given in Fig. 1f. All spectra show two obvious peaks, the G band with E_{2g} symmetry ascribed to ordered sp^2 carbon at around 1595 cm^{-1} and the D band with A_{1g} symmetry at about 1310 cm^{-1} ascribed to disordered carbon, edge defects, and other defects (sp^3 bonded carbon, dangling bonds, vacancies, and topological defects) [19].

The charge/discharge curves of GNS and N-GNS present similar Li$^+$ intercalation/de-intercalation profiles (see Fig. 2a and b). The presence of the plateau at about 0.6 V is assigned to the formation of a solid-electrolyte-interphase (SEI) film [20,21]. The capacity of the potential region lower than 0.5 V is due to Li$^+$ intercalation into the graphene layers [22]. The absence of a potential plateau suggests electrochemically and geometrically nonequivalent Li$^+$ sites [22]. GNS shows a higher coulombic efficiency (44%) in the first cycle. In the
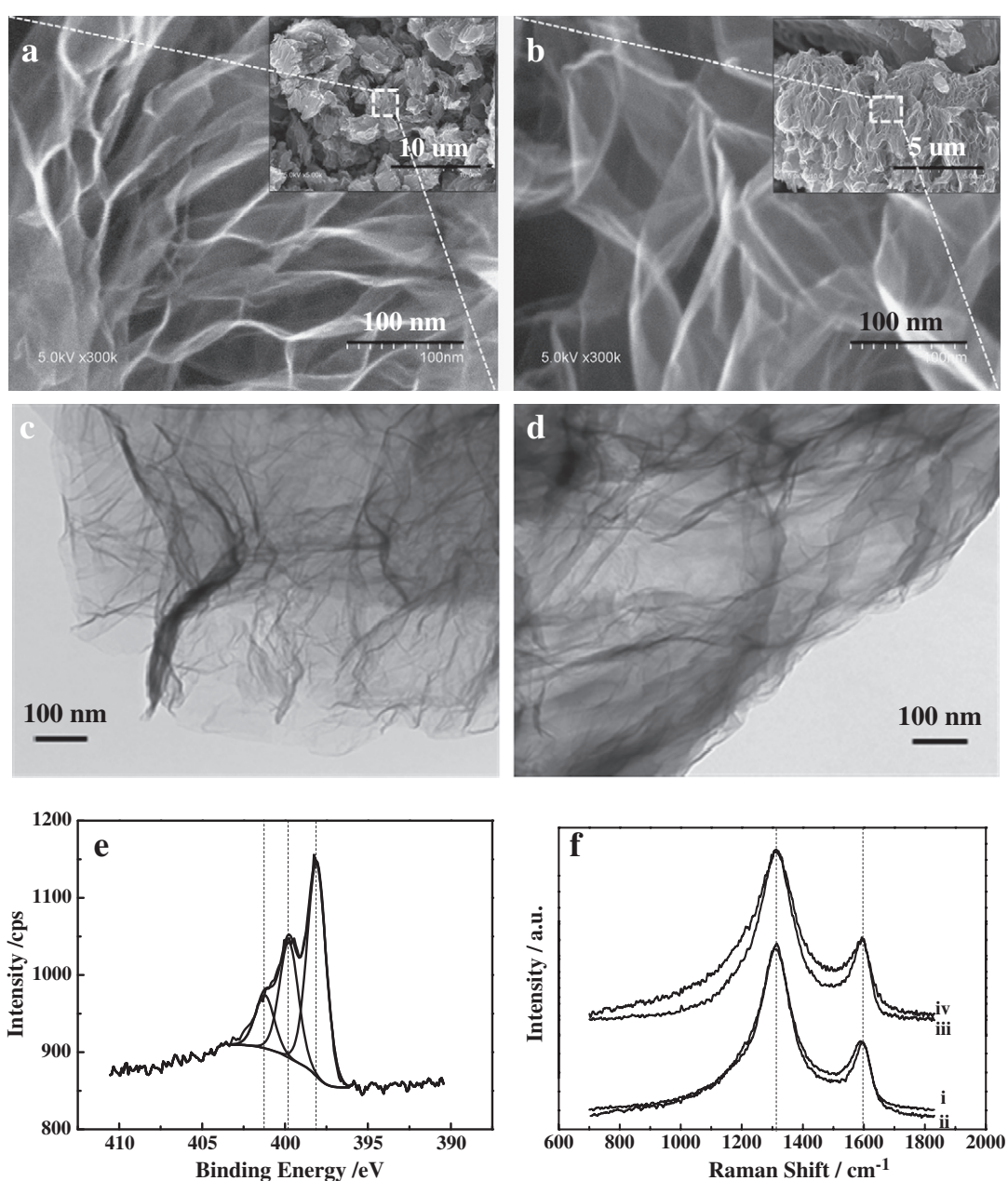

Fig. 1. SEM and TEM images of (a, c) GNS and (b, d) N-GNS; (e) XPS spectra of N 1 s fitting for N-GNS anode; (f) Raman spectra of GNS before (i) and after (ii) 100 cycles and N-GNS before (iii) and after (iv) 100 cycles.
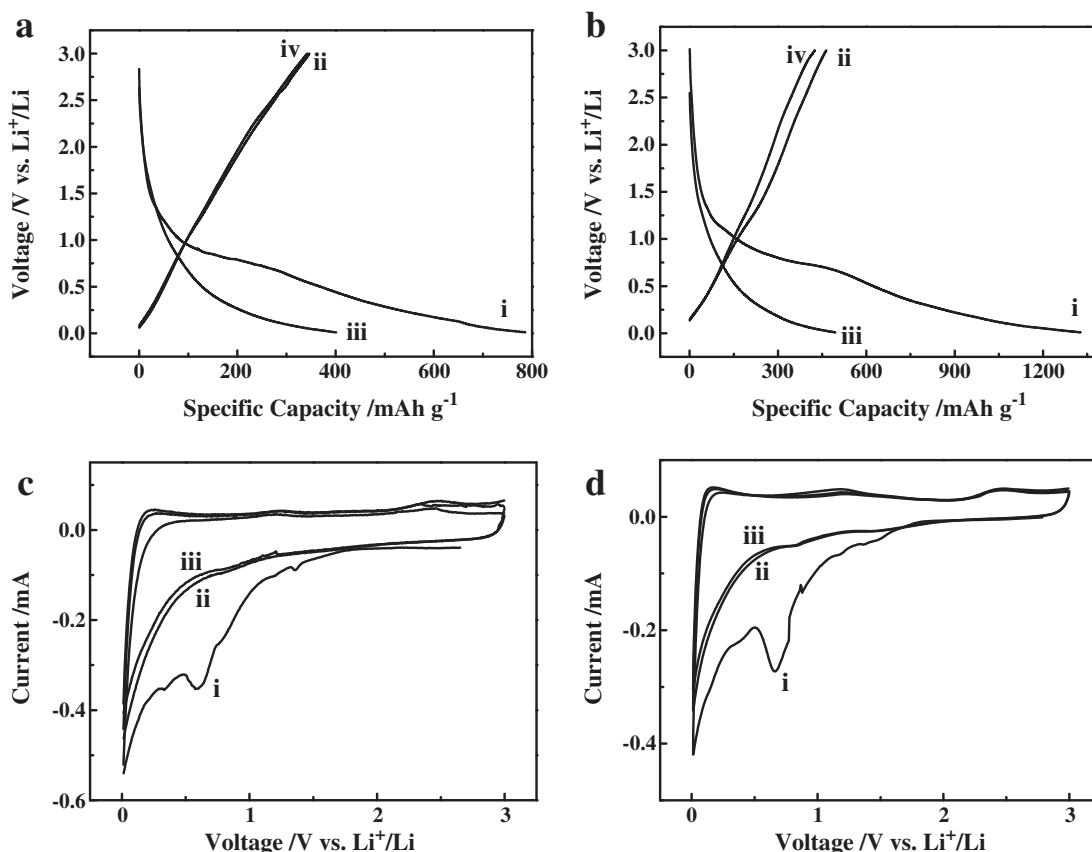
Fig. 2. Charge/discharge profiles: (i) the first discharge, (ii) the first charge, (iii) the second discharge, and (iv) the second charge; and cyclic voltammograms: (i) the first cycle, (ii) the second cycle, and (iii) the third cycle for (a, c) GNS and (b, d) N-GNS anodes.

case of N-GNS, in contrast, its coulombic efficiency is lower (37%), corresponding to a high irreversible capacity. The specific surface areas of GNS and N-GNS as measured by the N_2 absorption Brunauer–Emmett–Teller (BET) method are 456 m^2 g^{-1} and 599 m^2 g^{-1}, respectively. The larger specific surface area of N-GNS might be one of the reasons for its higher irreversible capacity due to SEI formation at the interface with the electrolyte.

In Fig. 2c and d, both GNS and N-GNS exhibit similar CV behaviors, showing that N-GNS has no obvious influence on the initial Li^+ intercalation/de-intercalation. The first reduction of both electrodes gives a prominent peak located at about 0.6 V due to the SEI films on the anodes. This peak disappears during the subsequent discharge, which is attributed to the isolation between the anodes and electrolyte due to the dense SEI film formed on the surface of the anodes in the first discharge. A peak close to 0 V was also observed in the CV curves resulting from Li^+ intercalation into the carbon based anodes. The difference of CV curves in the first two cycles and the similarity in the second and the third cycles indicate that the irreversible capacity losses of GNS and N-GNS mainly occur in the first cycle.

The cycling stability of GNS and N-GNS is presented in Fig. 3a. GNS shows regular cycling performance, gradually declining in the specific capacity with increasing charge/discharge cycles. The reversible discharge capacity after 100 cycles is 269 mAh g^{-1}, revealing 66% retention of the second cycle capacity. For N-GNS, a higher discharge capacity of 454 mAh g^{-1} is observed in the second cycle. In the first 17 cycles, its specific capacity decreases with cycles and shows the normal characteristics. Interestingly, as the cycling continued from the 17th cycle up to the 100th cycle, a significant increase in the specific capacity is observed from 364 mAh g^{-1} to 452 mAh g^{-1}. The

long-cycle vs. specific capacity plot for N-GNS is shown in Fig. 3b. Surprisingly, the specific capacity continues to increase, and reaches a maximum value (684 mAh g^{-1}) in the around 501st cycle and then remains constant. Obviously, N-GNS presents a superior cycle performance as anode for LIBs.

As it is shown in Fig. 1e, there are three types of nitrogen doping in the graphene framework. The pyridinic nitrogen atoms are two-coordinate N occurring on edges of graphene with a filled lone-pair orbital completing the trigonal sp^2 structure [23]. Its higher content is correlated with the lower degree of crystalline perfection [24] confirmed by Raman in Fig. 1f, which is beneficial to increasing the specific capacity of carbon based anodes. During the formation of pyridinic nitrogen, carbon vacancies are formed within a predominantly hexagonal graphene network [25]. These vacancies increase the Li^+ storage sites, resulting in the capacity increase of the N-GNS anode [26]. On the other hand, as it is shown in Fig. 1f, there is a large difference in the Raman spectra of N-GNS before and after 100 cycles, whereas it is similar for GNS. To compare the structural changes before and after 100 cycles, a critical factor of (I_D/I_G) is the integrated intensity ratio of the D band and G band [27]. The I_D/I_G value of GNS is 4.2 and 4.4 before and after 100 cycles, respectively. However, the I_D/I_G value of N-GNS increases from 4.8 to 8.0. The higher I_D/I_G value of N-GNS shows more disorder, more defects, and smaller sp^2 domains. Edges and other defects were suggested to store additional Li^+ in the graphite anode [28–30]. For N-GNS, the intensity growth of the disorder-induced D band (relative to the G band) indicates that Li^+ intercalation/de-intercalation into graphene sheets upon cycling brings about a more noticeable change in the degree of long-range ordering in the hexagonal lattice than that of GNS. N-GNS has a more disordered structure, including the generation of defects, with the
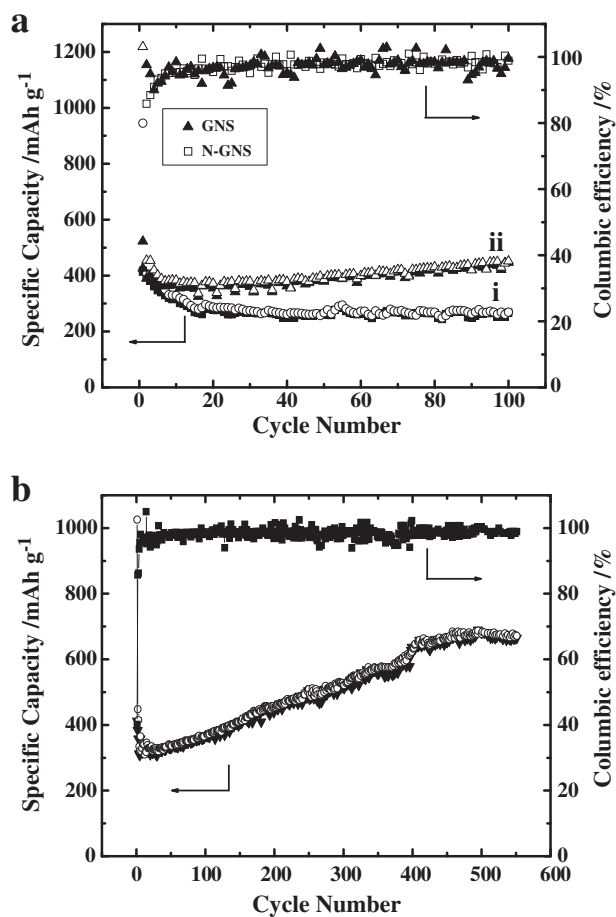
a

b

Fig. 3. (a) Reversible charge/discharge capacity verse cycle number of (i) GNS and (ii) N-GNS; (b) Superior cycle stability of the highest reversible capacity (684 mAh g^{-1} in the 501st cycle) of N-GNS in the long-run up to 550 cycles. (Hollow: discharge capacity; Solid: charge capacity).

charge/discharge process. These defect sites in N-GNS provide more Li$^+$ storage electrochemical active locations. Therefore, the capacity of N-GNS increases with cycles.

4. Conclusions

We have demonstrated that N-GNS has a superior specific capacity as anodes of LIBs in comparison to GNS. More interestingly, the charge/ discharge capacity of N-GNS increases with the charge/discharge cycles, reaching 684 mAh g^{-1} in the 501st cycle. The significant improvement

is due to the fact that the nitrogen introduction in the graphene plane leads to an increase in the number of defect sites and vacancies as Li$^+$ active sites on the surface of GNS. This study opens a door for using new nitrogen-doped graphene carbon nanostructures as anodes of LIBs.

Acknowledgements

References

[1] K.S. Novoselov, D. Jiang, F. Schedin, T.J. Booth, V.V. Khotkevich, S.V. Morozov, A.K. Geim, Proc. Natl. Acad. Sci. 102 (2005) 10451.
[2] K.S. Novoselov, A.K. Geim, S.V. Morozov, D. Jiang, Y. Zhang, S.V. Dubonos, I.V. Grigorieva, A.A. Firsov, Science 306 (2004) 666.
[3] M. Orlita, C. Faugeras, P. Plochocka, P. Neugebauer, G. Martinez, D.K. Maude, A.L. Barra, M. Sprinkle, C. Berger, W.A. de Heer, M. Potemski, Phys. Rev. Lett. 101 (2008) 267601.
[4] A.K. Geim, K.S. Novoselov, Nat. Mater. 6 (2007) 183.
[5] S.H. Lee, S.D. Seo, Y.H. Jin, H.W. Shim, D.W. Kim, Electrochem. Commun. 12 (2010) 1419.
[6] D.A.C. Brownson, C.E. Banks, Electrochem. Commun. 13 (2011) 111.
[7] X.C. Xiao, P. Liu, J.S. Wang, M.W. Verbrugge, M.P. Balogh, Electrochem. Commun. 13 (2011) 209.
[8] D. Pan, S. Wang, B. Zhao, M. Wu, H. Zhang, Y. Wang, Z. Jiao, Chem. Mater. 21 (2009) 3136.
[9] A.N. Kotov, Nature 442 (2006) 254.
[10] A.M. Rao, P.C. Eklund, Bandow Shunji, A. Thess, R.E. Smalley, Nature 388 (1997) 257.
[11] R.S. Lee, H.J. Kim, J.E. Fischer, A. Thess, R.E. Smalley, Nature 388 (1997) 255.
[12] M. Terrones, P.H. Redlich, N. Crobert, S. Trazobares, W.K. Hsu, H. Terrones, Y.Q. Zhu, J.P. Hare, C.L. Reeves, A.K. Cheetham, M. Ruhle, H.W. Kroto, D.R.M. Walton, Adv. Mater. 11 (1999) 655.
[13] Y.P. Wu, C.Y. Jiang, C.R. Wan, S.B. Fang, Y.Y. Jiang, J. Appl. Polym. Sci. 77 (2000) 1735.
[14] A.L.M. Reddy, A. Srivastava, S.R. Gowda, H. Gullapalli, M. Dubey, P.M. Ajayan, ACS Nano 4 (2010) 6337.
[15] W.S. Hummers, R.E. Offeman, J. Am. Chem. Soc. 80 (1958) 1339.
[16] D.S. Geng, Y. Chen, Y.G. Chen, Y.L. Li, R.Y. Li, X.L. Sun, S.Y. Ye, S. Knights, Energy Environ. Sci. 4 (2011) 760.
[17] X.R. Wang, X.L. Li, L. Zhang, Y. Yoon, P.K. Weber, H.L. Wang, J. Guo, H.J. Dai, Science 324 (2009) 768.
[18] J. Casanovas, J.M. Ricart, J. Rubio, F. Illas, J.M. Jimenez-Mateos, J. Am. Chem. Soc. 118 (1996) 8071.
[19] Y. Idota, T. Kubota, A. Matsufuji, Y. Maekawa, T. Miyasaka, Science 276 (1997) 1395.
[20] P. Guo, H.H. Song, X.H. Chen, Electrochem. Commun. 11 (2009) 1320.
[21] H. Zhou, S. Zhu, M. Hibino, I. Honma, M. Ichihara, Adv. Mater. 15 (2003) 2107.
[22] Z.H. Yang, H.Q. Wu, Mater. Lett. 50 (2001) 108.
[23] P.H. Matter, L. Zhang, U.S. Ozkan, J. Catal. 239 (2006) 83.
[24] H.C. Choi, J. Park, B.N. Kim, J. Phys. Chem. B 109 (2005) 4333.
[25] N.A. Kaskhedikar, J. Maier, Adv. Mater. 21 (2009) 2664.
[26] Y.P. Wu, S.B. Fang, W.G. Ju, Y.Y. Jiang, J. Power Sources 70 (1998) 114.
[27] H. Kim, J. Cho, Nano Lett. 8 (2008) 3688.
[28] M. Winter, J.O. Besenhard, M.E. Spahr, P. Novak, Adv. Mater. 10 (1998) 725.
[29] C. Menachem, E. Peled, L. Burstein, Y. Rosenberg, J. Power Sources 68 (1997) 277.
[30] E. Buiel, A.E. George, J.R. Dahn, J. Electrochem. Soc. 145 (1998) 2252.